
Article:
Howes, NUM orcid.org/0000-0002-4335-8593, Mir, ZS, Blitz, MA orcid.org/0000-0001-6710-4021 et al. (4 more authors) (2018) Kinetic studies of C_1 and C_2 Criegee intermediates with SO_2 using laser flash photolysis coupled with photoionization mass spectrometry and time resolved UV absorption spectroscopy. Physical Chemistry Chemical Physics, 20 (34). pp. 22218-22227. ISSN 1463-9076

https://doi.org/10.1039/c8cp03115k

Kinetic Studies of C_1 and C_2 Criegee Intermediates with SO_2 using Laser Flash Photolysis coupled with Photoionization Mass Spectrometry and Time Resolved UV Absorption Spectroscopy

N.U.M Howes[1], Z.S. Mir[1], M.A. Blitz[1,2]* S. Hardman[1], T.R. Lewis[1], D. Stone[1] and P.W. Seakins[1,2]*

1 - School of Chemistry, University of Leeds, Leeds, LS2 9JT, UK

2 – National Centre for Atmospheric Science, University of Leeds, Leeds, LS2 9JT, UK.

Abstract

Recent, direct studies have shown that several reactions of stabilized Criegee intermediates (SCI) are significantly faster than indicated by earlier indirect measurements. The reaction of SCI with SO_2 may contribute to atmospheric sulfate production, but there are uncertainties in the mechanism of the reaction of the C_1 Criegee intermediate, CH_2OO, with SO_2.

The reactions of C_1, CH_2OO, and C_2, CH_3CHOO, Criegee intermediates with SO_2 have been studied by generating stabilized Criegee intermediates by laser flash photolysis (LFP) of RI_2/O_2 (R=CH_2 or CH_3CH) mixtures with the reactions being followed by photoionization mass spectrometry (PIMS). PIMS has been used to determine the rate coefficient for the reaction of CH_3CHI with O_2, $k = (8.6 \pm 2.2) \times 10^{-12}$ cm^3 molecule^{-1} s^{-1} at 295 K and 2 Torr (He). The yield of the C_2 Criegee intermediate under these conditions is 0.86 ± 0.11. All errors in the abstract are a combination of statistical at the 1σ level and an estimated systematic contribution.

For the $CH_2OO + SO_2$ reaction, additional LFP experiments were performed monitoring CH_2OO by time-resolved broadband UV absorption spectroscopy (TRUVAS). The following rate coefficients have been determined at room temperature ((295 ± 2) K):

$CH_2OO + SO_2$: $k = (3.74 \pm 0.43) \times 10^{-11}$ cm^3 molecule^{-1} s^{-1} (LFP/PIMS),

$k = (3.87 \pm 0.45) \times 10^{-11}$ cm^3 molecule^{-1} s^{-1} (LFP/TRUVAS)

$CH_3CHOO + SO_2$: $k = (1.7 \pm 0.3) \times 10^{-11}$ cm^3 molecule^{-1} s^{-1} (LFP/PIMS)

LFP/ PIMS also allows for the direction observation of CH_3CHO production from the reaction of CH_3CHOO with SO_2, suggesting that SO_3 is the co-product. For the reaction of CH_2OO with SO_2 there is no evidence of any variation in reaction mechanism with [SO_2] as had been

suggested in an earlier publication (Chhantyal-Pun et al. PCCP, 17, 3617, 2015). A mean value of $k = (3.76 \pm 0.14) \times 10^{-11}$ cm^3 $molecule^{-1}$ s^{-1} for the $CH_2OO + SO_2$ reaction is recommended from this and previous studies. The atmospheric implications of the results are briefly discussed.

Introduction

Gas phase Criegee intermediates, CR_2OO (where R = H or alkyl radical), can be formed in the atmosphere from alkene ozonolysis and can act as an additional oxidant to OH and ozone. Methods of generating and directly observing Criegee intermediates have recently led to a number of studies (e.g. refs[1-4]) of Criegee species with atmospherically relevant compounds. These studies have shown that many rate coefficients are significantly higher than earlier, indirect studies had indicated.[5] Criegee chemistry has recently been reviewed in several articles.[4, 6-8] There is particular interest in the reactions of Criegee intermediates with SO_2 since these may act as additional oxidation processes for sulfate formation, especially in environments with high biogenic alkene emissions, and hence significant concentrations of Criegee intermediates.[9] Welz et al.[3] utilized the laser flash photolysis (LFP) of CH_2I_2 (R1) in the presence of oxygen to generate CH_2OO and monitored its removal via photoionization mass spectrometry (PIMS). At the low pressures used in these experiments, reaction R2a dominates CH_2I consumption.[10-12]

$$CH_2I_2 + h\nu \rightarrow CH_2I + I \qquad \text{(R1)}$$

$$CH_2I + O_2 \rightarrow CH_2OO + I \qquad \text{(R2a)}$$

$$CH_2I + O_2 + M \rightarrow ICH_2O_2 + M \qquad \text{(R2b)}$$

A room temperature (298 K) rate coefficient, $k_3 = (3.9 \pm 0.7) \times 10^{-11}$ cm^3 molecule^{-1} s^{-1}, was determined for the reaction of CH_2OO with SO_2 at pressures of ~4 Torr.[3] This determination of k_3 was orders of magnitude greater than that reported by earlier indirect studies.[5]

$$CH_2OO + SO_2 \rightarrow HCHO + SO_3 \qquad \text{(R3)}$$

Subsequently, Stone et al.[13] used the same method to generate CH_2OO, but followed the reaction by laser induced fluorescence of formaldehyde, HCHO over the pressure range 50 - 450 Torr of nitrogen. A pressure independent value of $k_3 = (3.40 \pm 0.41) \times 10^{-11}$ cm^3 molecule^{-1} s^{-1} was determined at 295 K which was in good agreement with experiments where CH_2OO removal was directly monitored via PIMS at a pressure of 1.5 Torr. The good agreement between rate coefficients determined by HCHO monitoring and PIMS studies of CH_2OO removal suggests that HCHO, and hence SO_3, are products of reaction R3. Recently,

Wang et al.[14] have reported the direct observation of SO_3 as the dominant product of reaction R3 in flash photolysis studies, confirming its potential atmospheric importance in sulfate production. Further studies on reaction R3 have been carried by Liu et al.[15], monitoring CH_2OO via laser induced fluorescence of OH, produced from the decomposition of CH_2OO (k_3 = (3.53 ± 0.29) × 10^{-11} cm^3 $molecule^{-1}$ s^{-1}), and by Sheps who monitored CH_2OO directly via time-resolved UV absorption spectroscopy (k_3 = (4.1 ± 0.3) × 10^{-11} cm^3 $molecule^{-1}$ s^{-1}).[16] Both studies used reactions R1 and R2 to generate CH_2OO and were able to monitor reaction R3 over a wide range of pressures at room temperature confirming the measurements of both Welz et al. and Stone et al.

Recent studies have raised questions about both the relevance of reactions of Criegee intermediates with trace atmospheric species and the mechanism of the reaction of CH_2OO with SO_2. Whilst the rate coefficient for the reaction of CH_2OO with water appears to be too slow to contribute to CH_2OO loss in the atmosphere, studies where CH_2OO could be monitored at high pressure (and hence higher [H_2O]), have shown a quadratic dependence of the rate coefficient for CH_2OO removal with [H_2O] indicating reaction with the water dimer rather than monomer.[17-24] The value of the rate coefficient with water dimer at 295 K, k = (4.0 ± 1.2) × 10^{-12} cm^3 $molecule^{-1}$ s^{-1},[18] suggests that this reaction should dominate CH_2OO removal under atmospheric conditions and, if applicable to higher Criegee intermediates, would limit the overall impact of Criegee chemistry in the atmosphere. However, C_2 Criegee intermediates can exist in two conformers, as shown in Figure 1, with a significant barrier of ~160 kJ mol^{-1} to interconversion.[25] The anti- conformer reacts rapidly with water or water dimer, via the formation of a ring structure involving the O and H atoms on the same side of the conformer, but the syn- conformer reacts much more slowly and therefore syn-C_{2+} Criegee intermediates may be available to react with trace atmospheric species.[1]

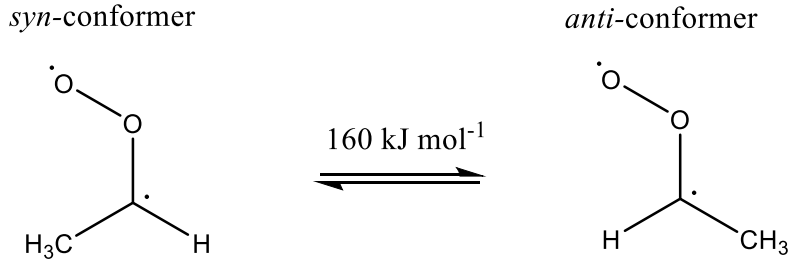

Fig. 1 Syn and anti-conformers of the C_2 Criegee intermediate.

Reaction R3 is probably the most well characterised C_1 Criegee intermediate reaction and is potentially fast enough to compete with CH_2OO removal by the water dimer, but recent measurements raise some controversy as to the mechanism of reaction. In 2015 Chhantyal-Pun et al.[26] directly monitored CH_2OO and, at high concentrations of SO_2 (> 7×10^{12} molecule cm^{-3}), determined a value for k_3 in good agreement with other recent studies. However, at low concentrations of SO_2 (< 7×10^{12} molecule cm^{-3}), where CH_2OO reacted under mixed first and second order kinetics, an enhanced CH_2OO removal was observed compared to the expected removal based on the rate coefficient determined at high [SO_2] and the CH_2OO self-reaction. Chhantyal-Pun et al. attributed this observation to a complex forming process of CH_2OO with SO_2 which increases the observed rate coefficient by nearly a factor of two to $k_3 = (7.46 \pm 0.29) \times 10^{-11}$ cm^3 $molecule^{-1}$ s^{-1}. Liu et al.[23] have recently studied reaction R3 using the indirect LIF method. The rate coefficient determined, $k_3 = (3.88 \pm 0.13) \times 10^{-11}$ cm^3 $molecule^{-1}$ s^{-1}, is in good agreement with previous measurements, but no measurements were made below [SO_2] ~ 5×10^{12} molecule cm^{-3}.

In this current work, studies using LFP of RI_2/O_2 (R = CH_2 and CH_3CH) to generate Criegee intermediates, and PIMS or UV absorption spectroscopy to monitor Criegee intermediates (and, where possible, products), have been carried out in order to address these issues. Earlier studies from this laboratory on the reaction of CH_2OO with SO_2 have been re-visited, particularly focusing on extending measurements to low concentrations of SO_2. Depending on atmospheric conditions, reaction R3 may be important in atmospheric oxidation processes and is important in interpreting chamber studies, particularly under low humidity conditions.

As discussed above, syn-C_2 Criegee intermediates may be available to react with trace atmospheric species and therefore we have measured the rates of reaction of CH_3CHOO with SO_2, monitoring the removal of CH_3CHOO and additionally following the time dependence of the product CH_3CHO. CH_3CHOO is generated from CH_3CHI_2 via an analogous mechanism to CH_2OO and additional studies have been carried out to quantify CH_3CHOO production both in terms of the kinetics of the reaction of CH_3CHI with O_2 and the I atom (and hence CH_3CHOO) yield. The PIMS apparatus in this study[27, 28] operates with a fixed photoionization energy, 10.5 eV, which ionizes both conformers of the C_2 Criegee intermediate. The tuneable photoionization apparatus used by Taatjes et al.[1] was able to selectively monitor the two

conformers showing that the syn-conformer is predominantly formed in the reaction of $CH_3CHI + O_2$ (~90%). Thus the results obtained in this study refer to the syn conformer and can be compared with those of other conformer specific studies such as those based on selective observations by time resolved UV absorption spectroscopy by Sheps et al.[29]

Experimental and Data Analysis

The studies were carried out at room temperature ((295 ± 2) K) using laser flash photolysis (LFP), coupled to either photoionization mass spectroscopy (PIMS) or time resolved broadband UV absorption spectroscopy (TRUVAS). The LFP/PIMS apparatus has been described before in detail.[27, 28, 30] Radicals were generated by laser photolysis at 248 nm (Lambda Physik Compex 102, 10 Hz, typically 8×10^{16} photons cm^{-2}) in a flow tube maintained at a total pressure of 1 – 2.5 Torr of helium. Mixtures of di-iodo precursor (1-10 × 10^{13} molecule cm^{-3}), oxygen (1-10 × 10^{13} molecule cm^{-3}, BOC 99.999%), SO_2 (Sigma-Aldrich, 99.9%) and helium (BOC, 99.999%) were premixed and introduced into the flow tube. Substrate and helium flows were controlled through calibrated mass flow controllers (MFC). Di-iodo compounds can be lost in the MFC and so were introduced from a thermostatted bubbler, located after the MFC, delivering a known helium flow to the bubbler, and controlled by a needle valve. Concentrations of the di-iodo species were determined from known vapour pressures at the bubbler temperature. Criegee intermediates were generated via reactions R1 and R2 (or the C_2 equivalents). Based on values presented above, the typical initial concentration of Criegee intermediates is estimated to be ($\sigma = 1.6 \times 10^{-18}$ cm^2, photon flux = 8×10^{16} photons cm^{-2}, $[CH_2I_2] = 1 \times 10^{13}$ molecule cm^{-3}) ~1.3×10^{12} molecule cm^{-3}. Oxygen concentrations were maintained such that Criegee intermediates were generated on a timescale that was fast ($\tau_2 \approx 5 \times 10^{-5}$ s) compared to their removal.

Reaction mixtures were sampled through a 1 mm hole in the side of the flow tube into a low pressure photoionization chamber where the mixture was photoionized by 118 nm light (equivalent to 10.5 eV). Ions were focused into a time of flight mass spectrometer (ToF-MS, Kore Instruments). 118 nm light was generated by focusing 355 nm radiation generated from a Nd-YAG laser (Continuum Precision II, 10 Hz, 25 mJ $pulse^{-1}$) into a glass cell containing 50 Torr of Kr and coupled directly into the photoionization chamber through a MgF_2 window.

The time-resolved mass signals (e.g. m/z = 46 or 60 for CH_2OO and CH_3CHOO) were detected using ToF-MS and tracked with an oscilloscope (LeCroy Wave-Runner), which then captured and integrated the signal. For each individual experiment a time-resolved scan consisting of 200 to 500 data points was collected over a timescale of 1-10 ms. These kinetic traces were averaged 10-20 times to increase the signal-to-noise ratio of the data. The inset to Figure 2 shows a typical example of a Criegee intermediate decay. The traces comprise of a fast rise in Criegee signal due to a combination of chemical production from reactions R1 and R2 and effusive transport, followed by a decay, attributed to reaction with SO_2. Each individual trace was analysed using OriginPro graphical software; the signal from the mass spectrometer was fitted using equations E1-3, using reaction R2 and R3 as an example.

$$M_1 = \frac{(S_{\mathrm{C1height}} \times k'_2 \times k_{\mathrm{eff}})}{(k'_3 - k'_2)} \quad \text{(E1)}$$

$$M_2 = \frac{e^{-k'_2 \times t} - e^{-k_{\mathrm{eff}} \times t}}{(k_{\mathrm{eff}} - k'_2)} - \frac{e^{-k'_3 \times t} - e^{-k_{\mathrm{eff}} \times t}}{(k_{\mathrm{eff}} - k'_3)} \quad \text{(E2)}$$

$$S_{\mathrm{CI}} = M_1 \times M_2 + S_{\mathrm{bg}} \quad \text{(E3)}$$

Here S_{CI} is the time-resolved Criegee intermediate signal; $S_{C1height}$ is the maximum height of S_{CI}; k'_2 is the rate coefficient for Criegee intermediate formation from reaction R2; k'_3 is the total loss rate coefficient of the Criegee intermediate where k'_3 is the sum of the pseudo-first order rate coefficient for reaction R3 ($k_3[SO_2]$) and k_{other}, the other Criegee intermediate loss processes (wall loss, self-reaction etc); k_{eff} is the rate coefficient for gas effusion through the pinhole (k_{eff} was determined in previous work[27] and held constant during data analysis, $k_{eff} = 20000\ s^{-1}$); t is time; and S_{bg} represents the background signal measured for the individual data traces. Further details on the analysis and the contribution of k_{eff} can be found in the SI (Section 2), Baez-Romero et al.[27] or Taatjes.[31] Plots of k'_3 vs $[SO_2]$ as shown in Figure 2 give the bimolecular rate coefficient, k_3, as the gradient and k_{other} as the intercept. Not all the contributions to k_{other} are pseudo-first order and hence constant for the different traces used to compile Figure 2. However, both experiments and simulations (see SI Section 1) have shown that the contribution of second order processes to k_{other} is negligible and a constant value for k_{other} is a good approximation.

The absorption experiments were carried out using our newly constructed multiplexing absorption kinetics spectrometer coupled to laser flash photolysis at (295 ± 2) K and 50 Torr (N_2). Full details about the setup can be found in a recent publication.[32] The essential details are as follows: the output from a laser driven xenon lamp (Energetiq, LDLS EQ-99X) was multi-passed 7 times through the 1.5 metre reaction cell and configured such that the probe beam was overlapped for (443 ± 21) cm with the 248 nm excimer laser beam that passed along the central length of the reactor. The probe beam was then directed via a fibre optic into a spectrograph (Jobin Yvon CP140-103) where the signals at wavelengths 250 – 850 nm were simultaneously detected using a CCD image sensor (Hamamatsu S7031, back-thinned FFT-CCD) with wavelength resolution of 1.54 nm (FWHM) at 313 nm. A 248 nm long-pass edge filter (248 nm RazorEdge) was used to prevent laser radiation entering the fibre optic. Signals at all wavelengths were recorded for 1 millisecond intervals for a total of 2000 milliseconds, where the excimer laser was fired after a 1000 milliseconds. These data were transferred in real time to a PC via a PCI interface board operating at 1 kHz (thus determining the 1 ms time resolution of the experiment). These data were processed by a PC using a custom built LabView program before the next photolysis laser pulse; the excimer laser was fired at 1/6 Hz to ensure minimal photolysis of reaction products from the previous photolysis pulse (residence time in the reactor is 4 s). At each wavelength, λ, the signal recorded at 1000 points before the excimer laser pulse were averaged and assigned to $I_0(\lambda)$ (intensity of the probe light), and each $I_0(\lambda)$ was compared to each of the wavelength-time points after the excimer laser fired, $I(\lambda,t)$. The program calculated $\Delta I/I_0$ for each wavelength and time point, giving the time-resolved absorption signal for each wavelength.

The observed time-resolved absorption spectra (examples of which can be seen in Lewis et al.[18]) obtained following photolysis of $CH_2I_2/O_2/N_2$ contained contributions from the CH_2I_2 precursor (contributing a constant and negative ΔI owing to its depletion on photolysis), CH_2OO and IO (generated by secondary chemistry). At long times post-photolysis (> 200 ms), contributions from CH_2OO were minimal owing to removal of CH_2OO from the system (primarily via R3), and the observed spectra contained contributions from only CH_2I_2 and IO. At wavelengths above 400 nm, the observed spectra at long times post-photolysis were thus dominated by IO absorbance, and a reference spectrum for IO was obtained for the wavelength grid and resolution of this experiment. This reference spectrum was then scaled to the observed

IO absorption peaks in the wavelength region 410-440 nm and subtracted from each absorption spectrum recorded at 1 ms intervals throughout the reaction, leaving time-resolved spectra containing contributions to the absorbance from only CH_2I_2 and CH_2OO. The CH_2OO spectrum was subsequently obtained in a similar manner to that described by Ting et al.[33], i.e. by subtracting an IO-subtracted absorption spectrum at a late time point (200 ms) following photolysis (which contains only the CH_2I_2 contribution owing to complete removal of CH_2OO through bimolecular reactions) from an IO-subtracted absorption spectrum at an early time point (5 ms) following photolysis (which contains both CH_2I_2 and CH_2OO contributions).

While absolute CH_2OO absorption cross-sections can be determined in these experiments, for the kinetics experiments reported in this work, absolute concentrations are not required. The normalised absorption spectra for CH_2OO, CH_2I_2 and IO, determined as described above, were fitted to the observed time-resolved absorption spectra between 300 and 420 nm at each time point following photolysis to determine the change in the CH_2OO signal, which is then normalised to the maximum Δ I for CH_2OO at ~340 nm for that particular experiment.

Bimolecular rate coefficients were obtained by plotting k'_3 vs $[SO_2]$ as shown in Figure 3 where the bimolecular rate coefficient is the gradient of the plot and the intercept accounts for loss processes of the Criegee intermediate that are independent of substrate (wall loss rate, decomposition, reaction with precursor).

Results and Discussion

a) Determination of the rate coefficient for the reaction $CH_2OO + SO_2$

The bimolecular rate coefficients for reaction R3 from this study, typified by the data shown in Figures 2 (PIMS) and 3 (TRUVAS) using two different techniques, are presented in Table 1. The errors presented in Table 1 are a combination of the statistical errors from the bimolecular plot at the 1σ level in combination with an estimated 10% systematic error (from uncertainties in flow rates, MFC calibrations etc). The consistency of the results obtained over a range of conditions (varying total pressure, different flowtubes and flow tube coatings for the PIMS studies) suggests that variations in these experimental parameters do not influence the

reaction. Over time, the wall loss rate in the PIMS experiments has been reduced making it easier to identify the enhancement of CH_2OO loss due to reaction with SO_2 and hence allowing the use of lower concentrations of SO_2. Averaging the determinations of experiments 1-5 for the bimolecular rate coefficient for reaction R3 gives $k_3 = (3.74 \pm 0.43) \times 10^{-11}$ cm^3 molecule^{-1} s^{-1} for the PIMS studies. Under the substrate and radical concentrations used in these studies, k_3 can be extracted using conventional pseudo-first-order analysis; the potential for complications from secondary reactions is investigated in Section 1 of the Supplementary Information. This value for k_3 is in good agreement with many of the recently measured values of k_3 as shown in Table 2.

Table 1: Rate coefficients, k_3, for the reaction of CH_2OO with SO_2 obtained from this study at (295 ± 2) K

Experiment	$[SO_2]$/molecule cm^{-3}	Flow tube	k_3 (10^{-11} molecule^{-1} cm^3 s^{-1})[a]
1	$(0.5 – 9.0) \times 10^{13}$	Coated[b]	3.62 ± 0.52
2	$(0.5 – 11.0) \times 10^{13}$	Uncoated	3.60 ± 0.41
3	$(0.5 – 11.0) \times 10^{13}$	Coated	4.02 ± 0.61
4	$(2.5 – 17.0) \times 10^{13}$	Coated	3.78 ± 0.40
5	$(0.5 – 7.5) \times 10^{13}$	Coated	3.70 ± 0.42
5a	$(0.5 – 2.5) \times 10^{13}$ [c]	Coated	3.65 ± 0.41
5b	$(0.5 – 1.5) \times 10^{13}$ [c]	Coated	3.46 ± 0.39
6	$(0.1 – 1.1) \times 10^{13}$	TRUVAS	3.87 ± 0.46

a Errors are a combination of statistical uncertainty from the bimolecular plot at the 1σ level and an estimated 10% systematic uncertainty, **b** Halocarbon wax, **c** These are the rate coefficients determined from a bimolecular plot using data from experiment 5, but over different $[SO_2]$ focusing on lower concentrations.

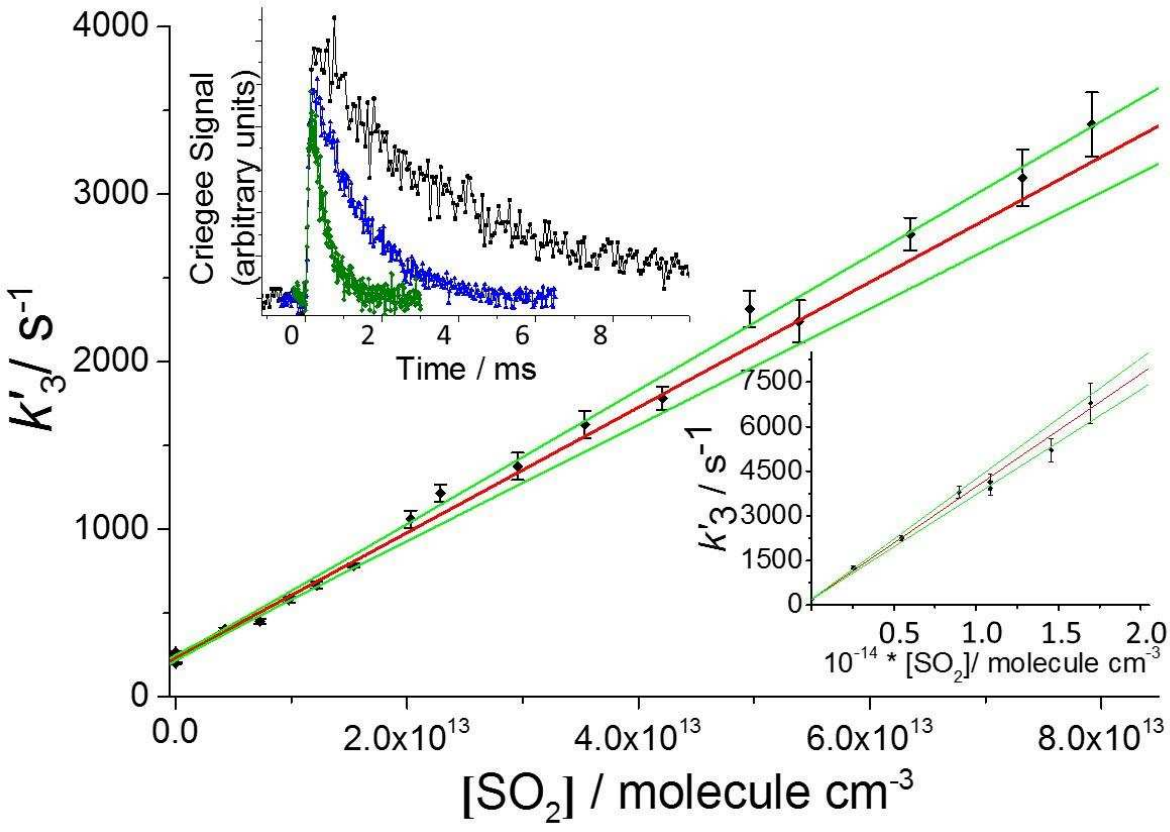

Fig. 2 Bimolecular plots of the $CH_2OO + SO_2$ reaction (R3) at 295 K and a total pressure of 2 Torr He using the PIMS method. The main figure shows data with $[SO_2]$ up to ~8 × 10^{13} molecule cm^{-3}. The red line is a weighted linear fit to the data (k_3=(3.73±0.13)×10^{-11} cm^3 $molecule^{-1}$ s^{-1}); the green lines are 1σ confidence bands; the error quoted is the statistical error. The upper inset shows typical CH_2OO temporal profiles at different $[SO_2]$ (black 0, blue 1.5 × 10^{13}, green 6.4 × 10^{13} molecule cm^{-3}) and the lower inset shows a bimolecular plot to higher concentrations of SO_2 (k_3=(3.78±0.11)×10^{-11} cm^3 $molecule^{-1}$ s^{-1}).

Figure 3 shows a bimolecular plot obtained from the TRUVAS studies with concentrations of SO_2 ranging from (0.1 – 1.1) × 10^{13} molecule cm^{-3} with an example of a typical absorption profile shown in the inset. The resultant value of the weighted bimolecular rate coefficient, k_3 = (3.87 ± 0.45) × 10^{-11} cm^3 $molecule^{-1}$ s^{-1} (where the error represents a combination of the statistical error and an estimated systematic error of 10%), is in agreement with the LFP/PIMS studies and includes the low $[SO_2]$ where Chhantyal-Pun et al. observed enhanced reactivity. The error reported in these studies is a combination of the statistical error (1σ) in the bimolecular plot (6%) combined with an estimated 10% systematic uncertainty. In addition to a bimolecular analysis, we have also performed a global analysis, treating the data either as a mixed order decay with a contribution from the Criegee self-reaction, or as a first

order process. For the mixed order analysis, the returned values for k_3 (3.49 – 3.56 × 10^{-11} cm^3 $molecule^{-1}$ s^{-1}) were insensitive to the value chosen for the rate coefficient of the Criegee self-reaction which was varied from 1 – 100 × 10^{-12} cm^3 $molecule^{-1}$ s^{-1}, demonstrating that, as expected, the self reaction was not contributing at the low concentrations of Criegee radicals used in our TRUVAS experiments ($[CH_2OO]_0$ = 1 – 5 × 10^{11} molecule cm^{-3}).

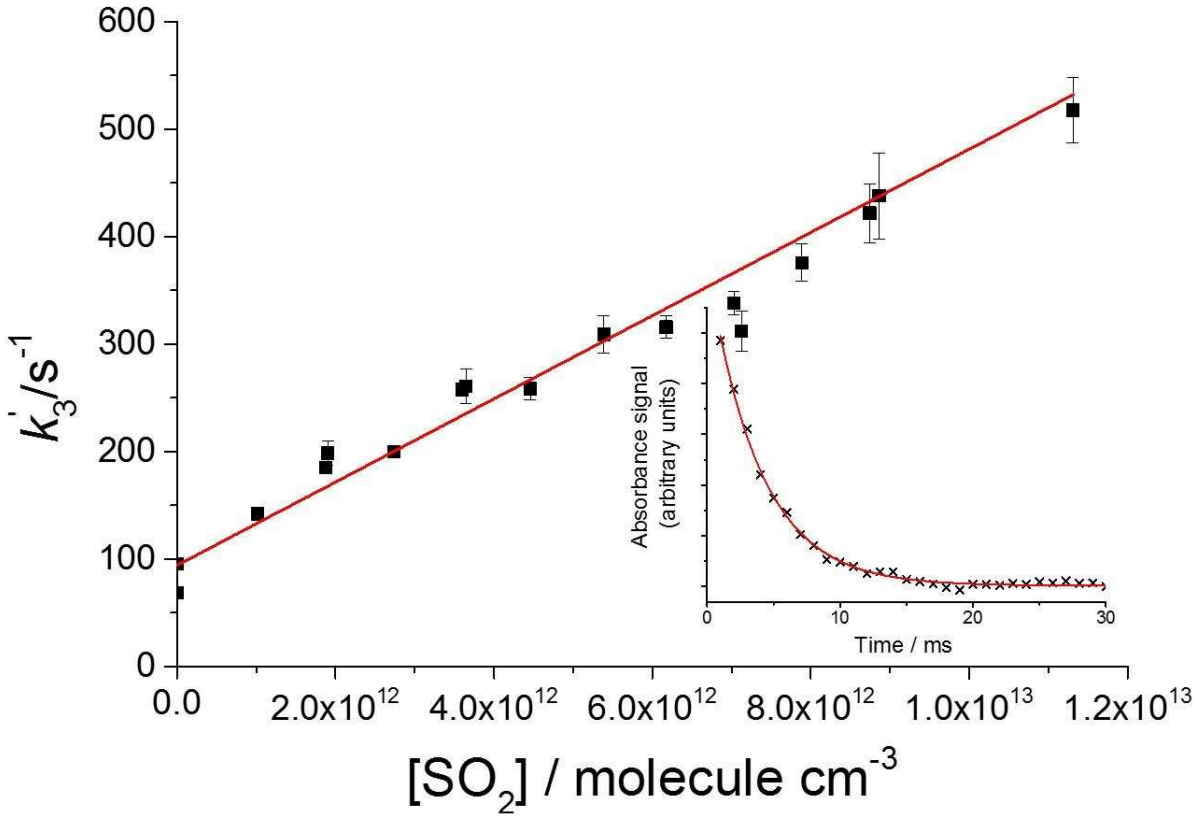

Fig. 3 Bimolecular plot for reaction R3 obtained using laser flash photolysis coupled with TRUVAS detection of CH_2OO. The resulting bimolecular rate coefficient is (3.87 ± 0.22) × 10^{-11} cm^3 $molecule^{-1}$ s^{-1} where the errors represent the statistical error (1σ) from the bimolecular fit (~6%). The inset shows a typical decay profile where the trace represents the Criegee signal determined from fitting spectra for CH_2I_2, IO and CH_2OO to the observed time-resolved absorption spectra between 300 and 420 nm, normalised to the peak Criegee absorption at ~340 nm, as described in the main text. For this trace, $[SO_2]$ = 4.5 × 10^{12} molecule cm^{-3}.

Table 2: Literature values for k_3 determined with a range of experimental techniques.

Reference	Technique	Pressure /Torr	$[SO_2]/10^{13}$ molecule cm^{-3}	$k_3 / 10^{-11}$ cm^3 $molecule^{-1}$ s^{-1}
Johnson et al. 2001[34]	GC-FID[a]	760 (Air)	1000	0.0004 ± 0.0001
Welz et al. 2012[3]	LFP (248 nm)[b]/PIMS[c]	4 (He)	0.4 – 4.5	3.9 ± 0.7
Stone et al. 2014[13]	LFP (248 nm)/LIF[d] H_2CO LFP (248 nm)/PIMS	500 (N_2) 1.5 (He)	20 – 120 1 – 9	3.42 ± 0.50
Liu et al. 2014[15]	LFP (351 nm)/LIF[d] OH	200 (Ar)	0.1 – 0.9	3.53 ± 0.29
Sheps 2013[16]	LFP (266 nm) /TRUVAS[e]	5 (He)	0.5 – 3.0	4.1 ± 0.3
Chhantyal-Pun et al. 2015[26]	LFP (355 nm)/CRDS[f]	30 (N_2)	2 - 12 0 – 2	3.80 ± 0.04 7.46 ± 0.29
Huang et al. 2015[35]	LFP (248 nm) /TRUVAS	30-756 (N_2)	2 - 12	3.57 ± 0.28
Liu et al. 2017[23]	LFP (355 nm) /LIF OH	10 (Ar)	0.6 – 2.5	3.88 ± 0.13
This Study	LFP (248 nm) /PIMS	2 (He)	0.5 - 17	3.74 ± 0.43[g,h]
This Study	LFP (248 nm) /TRUVAS	**(N_2)	0.1 – 1.1	3.87 ± 0.45[h]

a GC–FID = gas chromatography with flame ionization detection, **b** LFP = laser flash photolysis of CH_2I_2 in the presence of O_2, **c** PIMS = photoionization mass spectrometry monitoring CH_2OO, **d** LIF = laser induced fluorescence, **e** TRUVAS = time resolved ultra-violet absorption spectroscopy, monitoring CH_2OO, **f** CRDS = cavity ring down spectrometry, monitoring CH_2OO. **g** Average of LFP/PIMS studies. **h** Error is combination of statistical (1σ) and systematic errors.

Two measurements in Table 2 standout from the remainder of the data; the first is the indirect study of Johnson et al.[34] and possible explanations for the low value of k_3 determined in this study can be found in recent discussions.[13] The second is that reported by Chhantyal-Pun et al.[26] at low $[SO_2]$ (1×10^{12} molecule $cm^{-3} < [SO_2] < 7 \times 10^{12}$ molecule cm^{-3}), generating CH_2OO with a similar methodology as this work, but using 355 nm radiation to photolyse CH_2I_2, and monitoring the concentration of CH_2OO in real time using cavity ring down spectroscopy (CRDS). At high $[SO_2]$ ($2 – 22 \times 10^{13}$ molecule cm^{-3}), Chhantyal-Pun et al. reported $k_3 = (3.80 \pm 0.04) \times 10^{-11}$ cm^3 $molecule^{-1}$ s^{-1} in excellent agreement with this and other work (see Table 2). The authors attribute the enhanced removal of CH_2OO at low $[SO_2]$ using a complex forming mechanism. In this mechanism an SO_2-catalysed reversible isomerisation/intersystem crossing (ISC) reaction (R4, R-4) is in competition with the $CH_2OO + SO_2$ reaction (R3).

$$CH_2OO + SO_2 \rightarrow HCHO + SO_3 \qquad (R3)$$

$CH_2OO + SO_2 \rightleftharpoons$ Intermediate + SO_2 (R4, R-4)

Intermediate $\rightarrow$ Products (R5)

$CH_2OO \rightarrow$ loss via 1st and 2nd order processes (R6)

The impact this competition has on the overall reaction scheme was determined by invoking a steady state approximation, i.e. the rate of (R-4 + R5)>>R4, to the concentration of the intermediate product of this reaction. At high concentrations of SO_2: $k_{-4}[SO_2] >> k_5$, therefore the dominant loss mechanism of CH_2OO under these conditions is R3. However at low $[SO_2]$, $k_{-4}[SO_2] << k_5$, meaning that any of the intermediate formed will be quickly lost via reaction R5 and thus the reaction that forms the intermediate is the rate-determining step, R4. As a result of this, the rate of reaction under low $[SO_2]$ will be dependent upon k_4; specifically, the pseudo-first order loss of CH_2OO is $(k_3 + k_4)[SO_2]$ under such conditions. Thus the rate coefficient is increased by k_4 at low concentrations of SO_2, explaining the augmentation in the CH_2OO decay observed by Chhantyal-Pun et al.

As the concentration of SO_2 in the atmosphere is generally of the order of 1 - 50 ppb[36, 37] (i.e. in the low $[SO_2]$ region of the Chhantyal-Pun et al. study), it is important to verify this enhanced reactivity. Before commencing our PIMS studies on the loss of CH_2OO with low concentrations of SO_2, the decays of CH_2OO in the absence of any SO_2 were carefully examined. The decays were predominantly, but not purely first-order, suggesting that second-order CH_2OO recombination kinetics were also making a minor contribution to CH_2OO removal. Analysing with a mixed first and second order loss process allowed for a determination of the minor second-order loss component. Using an averaged value of 7.1×10^{-11} cm^3 $molecule^{-1}$ s^{-1} [26, 33, 38] for the CH_2OO self-reaction allowed an estimate for the initial concentration of CH_2OO, $[CH_2OO]_0$, to be calculated at 1.5×10^{12} molecule cm^{-3} (consistent with our estimates from photon flux and precursor concentration). Using the determined wall loss rates and our estimated $[CH_2OO]_0$, variations in the CH_2OO decays as a function of concentration of SO_2 were simulated. These simulations showed that pseudo first-order conditions were maintained down to $[SO_2] = 4.5 \times 10^{12}$ molecule cm^{-3} in the PIMS experiments. There will be uncertainties in this value due to correlations in mixed order fits of the decays in the absence of SO_2 and uncertainties in the self-reaction kinetics, but this estimate provides a

sensible lower bound for reliable extraction of k_3 from the PIMS studies. Further details can be found in the supplementary information.

The main bimolecular plot in Figure 2 shows k'_3 for $[SO_2]$ ranging from $5 \times 10^{12} - 7.5 \times 10^{13}$ molecule cm^{-3} using the PIMS technique (expt 5 in Table 1). From this plot there appears to be no variation in the rate coefficient with $[SO_2]$ and the bimolecular rate coefficient recorded, $k_3 = (3.70 \pm 0.42) \times 10^{-11}$ cm^3 $molecule^{-1}$ s^{-1}, is in agreement with other work in this study (see inset in Figure 2 showing bimolecular plot to higher $[SO_2]$, expt 4 in Table 1) and with several other studies. Additionally, the datasets have also been analysed with a global technique where all the decay traces are fitted simultaneously with a mixture of global parameters such as k_3 and k_{eff}, local parameters such as the signal height for each decay, and local information such as the $[SO_2]$ for each decay. Further details and example figures can be found in the supplementary information. Experiments 5a and 5b (Table 1) show the results of this global analysis for different concentration ranges of $[SO_2]$ focusing on lower concentrations of $[SO_2]$. There is good agreement with the results of the conventional analysis and no significant trend of k_3 with $[SO_2]$. The data on k_3 from the PIMS studies are supported by our TRUVAS studies which return a value of $k_3 = (3.87 \pm 0.45) \times 10^{-11}$ cm^3 $molecule^{-1}$ s^{-1} for low concentrations of SO_2 in the range $1 - 12 \times 10^{12}$ molecule cm^{-3} molecule cm^{-3}. Again, the data from the TRUVAS show no variation in the rate coefficient, k_3, as a function of $[SO_2]$ where the $[SO_2]$ range covers the switch between the two conditions of the Chhantyal-Pun et al. mechanisms.

It is difficult to reconcile the data from this study at low concentrations of $[SO_2]$ with the results of Chhantyal-Pun et al.[26] The high precision and quality of the data from Chhantyal-Pun et al. is such that the small differences in the mixed order decays (predominantly second-order at low $[SO_2]$) of CH_2OO could be reproducibly observed. However, simulations of the data of Chhantyal-Pun et al. (see SI Section 3) show that the changes in $[CH_2OO]$ associated with reaction R3 are small for a majority of the decay, i.e. most of the CH_2OO decay at low $[SO_2]$ is controlled by the self-reaction and the study is insensitive to k_3 under these conditions (see Fig S6a). Differences in the simulated decays for different values of k_3 only become more significant (still less than 20%) at longer times (see Fig S6b) where unknown complex chemistry (e.g. reactions of Criegee intermediates with the products of the self-reaction or of reaction R3) could be more prevalent and $[CH_2OO]$ is 30% or less of the starting value.

Additionally, Chhantyal-Pun et al. note that their mechanism is incompatible with the most recent potential energy surface of Vereecken et al.[39] as any intermediate, such as the singlet biradical or dioxirane, would be lower in energy than the Criegee species thus making it unlikely that the SO_2 catalysed isomerization (R4, R-4) will be in a steady-state. However, Vereecken et al. note that there are small (< 0.5 kJ mol^{-1}) singlet-triplet splittings, e.g. close in energy to the $OCH_2OS(O)O$ biradical intermediate, and Chhantyal-Pun et al. suggest this could promote intersystem crossing to the triplet surface in the presence of SO_2.

The combination of this work and other studies, which have used a wide range of detection methodologies, suggest that the mechanism of reaction R3 is independent of the concentration of sulfur dioxide and that at 295 K a mean pressure independent value of k_3 = $(3.76 \pm 0.14) \times 10^{-11}$ cm^3 $molecule^{-1}$ s^{-1} (from the two determinations of this work, the high $[SO_2]$ values of Chhantyal-Pun et al. and refs[3,10-12,19,26] and where the error represents 95% confidence limits), can be used in atmospheric modelling studies.

b) Yield of CH_3CHOO from the reaction of CH_3CHI with O_2 measured with LFP/PIMS

The C_2 Criegee intermediate was formed by reactions analogous to those used to generate CH_2OO:

$$CH_3CHI_2 + h\nu \rightarrow CH_3CHI + I \qquad (R7)$$

$$CH_3CHI + O_2 \rightarrow CH_3CHOO + I \qquad (R8a)$$

$$CH_3CHI + O_2 + M \rightarrow CH_3CHIO_2 + M \qquad (R8b)$$

Monitoring I atom production (at m/z 127) in the presence and absence of oxygen allows for the determination of the Criegee intermediate yield from reaction R8. In the absence of oxygen, photolysis leads to the rapid formation of a constant I atom signal (lower trace in the inset to Figure 4); the corresponding I atom concentration should be equal in magnitude to the concentration of CH_3CHI formed in the photolysis pulse. Addition of oxygen leads to the production of further I atoms from reaction R8a with the I atom signal reaching a new, higher concentration (upper trace in the inset to Figure 4). On the timescale of our studies I atoms are not lost via wall or recombination reactions. If reaction R8a accounted for 100% of CH_3CHI removal, then the I atom signal would double in the presence of excess oxygen. Analysis of the

long time (>1 ms) I atom signal using a first order fit, in the absence and presence of oxygen, directly yields the branching ratio of Criegee intermediate in reaction R8 which is determined as 0.86 ± 0.11 at 2 Torr of helium. The earlier studies of Stone et al.[12] to determine the yield of CH_2OO from reaction R2 used I atom resonance fluorescence to monitor I atom production and hence were able to operate over a wider range of pressures (5 – 450 Torr). A Stern Volmer analysis of CH_2OO production suggests a yield of CH_2OO close to unity at 2 Torr of He.[10, 12] For reaction R8, it might be expected that, because of the larger size of the activated CH_3CHIO_2* species formed in reaction R8 compared to ICH_2O_2* (formed in reaction R2), the unimolecular rate coefficient for decomposition to CH_3CHOO + I should be slower than the corresponding decomposition to CH_2OO, allowing for more stabilization toward reaction R8b. Stone et al. estimated an 18% yield of CH_2OO at 1 bar and therefore it is possible that biogenically active marine environments, where RI_2 emissions are significant, CH_2OO production may be relevant. However, by analogy, our results would suggest that CH_3CHOO production would be less likely. Determinations at higher pressures would be required to quantify atmospheric yields of CH_3CHOO production.

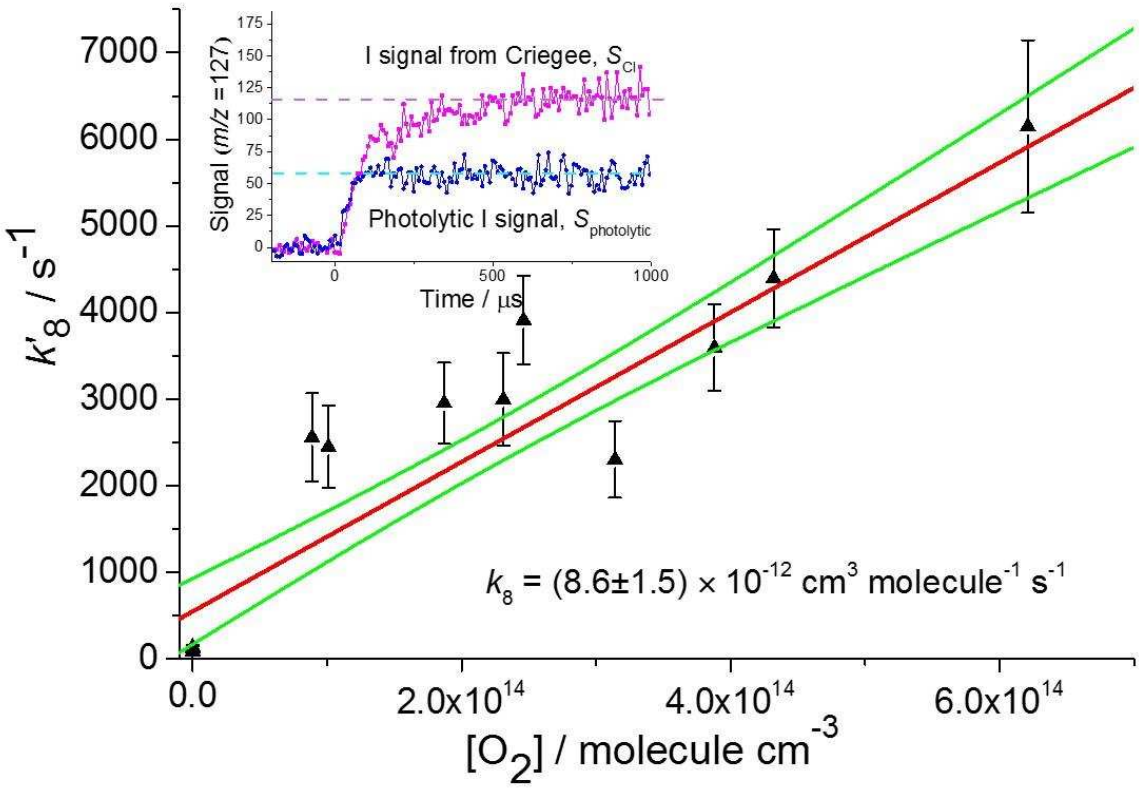

Fig. 4 Bimolecular plot of the $CH_3CHI + O_2$ reaction and a weighted fit to the data. The error quoted is from statistical errors at the 1σ level. The insert shows an example of an I atom experimental trace in the absence (blue) and presence (purple) of oxygen (6.1×10^{14} molecule cm^{-3}).

The kinetics of reaction R8 were monitored in the PIMS system by following the production of I atoms at m/z = 127 in the presence of varying excess concentrations of oxygen and the resulting bimolecular plot is shown in Figure 4. The rate coefficient for reaction R8 at ~1 Torr was determined as $k_8 = (8.6 \pm 2.2) \times 10^{-12}$ cm^3 molecule^{-1} s^{-1}. Here the error represents the statistical error (~15%) and a larger systematic error of 20%. The I atom signals have a long-time growth possibly due to IO recombination (formed in secondary chemistry following CH_3CHIO_2 recombination), which can be decoupled from the kinetics of R8, but increases the uncertainty of the analysis.

The rate coefficient for reaction R8 has only previously been measured by Sheps et al.[29], who reported $k_8 = (8.0 \pm 0.8) \times 10^{-12}$ cm^3 molecule^{-1} s^{-1} in good agreement with the current work. The value of the rate coefficient for the reaction of CH_3CHI with O_2 is significantly faster than the corresponding C_1 CH_2I reaction with O_2 (R2), $CH_2I + O_2 \rightarrow$ products; $k_2 = (1.67 \pm$

0.08) × 10^{-12} cm^3 $molecule^{-1}$ s^{-1} [12], (1.58 ± 0.22) × 10^{-12} cm^3 $molecule^{-1}$ s^{-1} [10], (1.6 ± 0.2) × 10^{-12} cm^3 $molecule^{-1}$ s^{-1} [40] and (1.40 ± 0.35) × 10^{-12} cm^3 $molecule^{-1}$ s^{-1} [41].

c) Determination of the rate coefficient for the reaction syn-CH_3CHOO + SO_2

Figure 5 shows the bimolecular plot for the study of CH_3CHOO with SO_2 (R9) obtained using LFP/PIMS with the same methods as for the LFP/PIMS study of R3.

$$CH_3CHOO + SO_2 \rightarrow \text{Products} \qquad \text{(R9)}$$

As mentioned above, the PIMS system used in this study is unable to differentiate between the syn and anti-conformers of CH_3CHOO, but the earlier work of Taatjes et al.[1] (syn:anti = 9:1) and Sheps et al.[29] (syn:anti = 3:1) suggests that our CH_3CHOO signal at m/z = 60 should be dominated by the syn-conformer. The signal to noise ratio for these studies (~3:1, see Figure 6) was lower than for the study of R3 (~10:1, see inset to Figure 2) as the lower volatility of the CH_3CHI_2 precursor compared to CH_2I_2 means that it was difficult to get the same precursor concentrations into the flow tube. The rate coefficient determined for reaction R9 at 1 – 2.5 Torr, k_9 = (1.7 ± 0.2) × 10^{-11} $molecule^{-1}$ cm^{-3} s^{-1}, with the error quoted to 1σ, is compared with the literature values shown in Table 3.

Table 3: Recent evaluations of k_9[a] from literature

Reference	Technique	Pressure /Torr	$[SO_2]/10^{13}$ molecule cm^{-3}	k_9 / 10^{-11} cm^3 s^{-1}
Taatjes et al.[1] (2013)	LFP/PIMS	4 (He)	1 - 5	2.4 ± 0.3[a]
Smith et al.[42] (2014)	LFP/TRUVA	15-100 (N_2)	155 - 600	2.0 ± 0.3
Sheps et al.[29] (2014)	LFP/TRUVA	20 (He)	0.8 – 4.8	2.9 ± 0.3[a]
This Work	LFP/PIMS	2 (He)	2 - 9	1.7 ± 0.3[b]

a – values are taken for the syn conformer if conformer specific data are available. b – Error is statistical error at the 1σ level combined with an estimate of systematic uncertainties

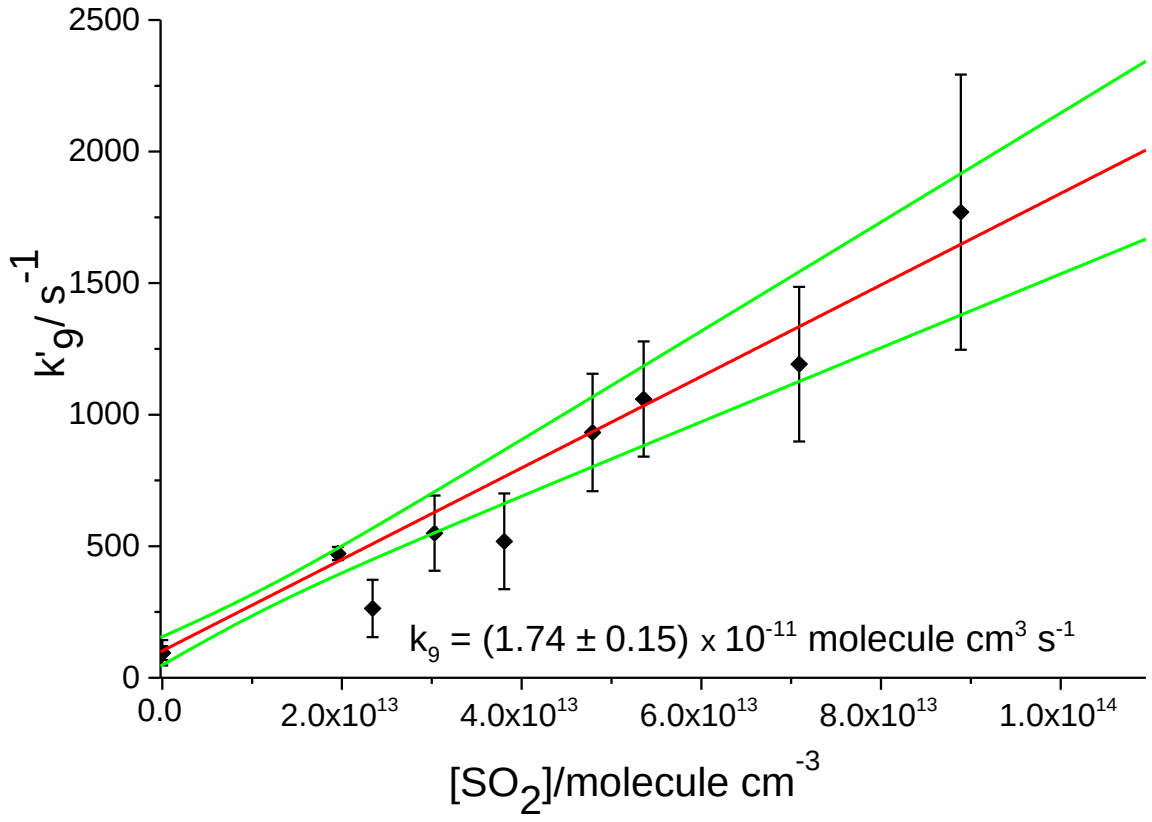

Fig. 5 A bimolecular plot of the reaction between CH_3CHOO and SO_2. The error quoted is propagated using the random errors quoted from the experiments at (1σ). An example of a CH_3CHOO decay trace is shown in Figure 6.

Our determination of k_9 is slightly lower than that of either Taatjes et al.[1] or Sheps et al.[29] but does overlap with the study of Smith et al.[42] All determinations report a lower value for the rate coefficient compared to CH_2OO, but only less than ~factor of two, such that if the rate coefficient for syn-CH_3CHOO with water or water dimer is sufficiently slow, then syn-CH_3CHOO could possibly contribute to atmospheric SO_2 oxidation. The conformer specific PIMS studies of Taatjes et al. reported similar rate coefficients for the reaction of the two conformers with SO_2 whereas the TRUVAS studies of Sheps et al.[29] report the anti conformer reacting almost a factor of 10 faster. Our studies measure an overall rate coefficient for both conformers present; if there is a significant difference in conformer reactivity, our low value for the rate coefficient suggests that syn-CH_3CHOO is the dominant conformer in our experiments.

From Figure 5 it can also be seen that the y-intercept of the plot is small (~150 s^{-1}); the y-intercept of the bimolecular plot (Figure 5) is equal to all of the C_2 Criegee intermediate loss processes, which includes wall losses, self-reaction and decomposition. Notably, this means the rate of decomposition, k_d, must be less than 150 s^{-1}; this is lower than the determination by Newland et al.[43] of (288±275) s^{-1} for the syn-conformer although the large error bars do overlap with our current estimate. Moreover, by analogy with the CH_2OO studies, the wall losses in the system are thought to contribute significantly to the value of the y-intercept, $k_{wall} \approx 50\ s^{-1}$. If this evaluation of k_{wall} is accurate, it suggests that the rate of decomposition must be less than $k_d \approx 50\ s^{-1}$; this estimate is of the same order as an earlier evaluation of $3 < k_d\ (s^{-1}) < 30$, made by Novelli et al.[44]

The contribution of CH_3CHOO to SO_2 oxidation in the atmosphere will depend on the products of reaction R9. Reactions of Criegee intermediates with SO_2 have been postulated to proceed via the formation of an excited ozonide species followed by decomposition to SO_3[39] and the corresponding carbonyl – the dominant route for C_1 Criegee intermediates, or stabilization.

$$CH_3CHOO + SO_2 \rightarrow CH_3CHO + SO_3 \qquad \text{(R9a)}$$

$$CH_3CHOO + SO_2 + M \rightarrow \text{Stabilized ozonide} \qquad \text{(R9b)}$$

A major advantage of using the PIMS set-up is that multiple species may be monitored simultaneously; whilst it is not possible to monitor either SO_3 or HCHO with our apparatus due to their inaccessible ionization potentials (IP), we can detect CH_3CHO (m/z = 44, IP = 10.22 eV[45]). Figure 6 shows the time dependence of the signals at m/z = 60 (CH_3CHOO) and 44 (CH_3CHO). There is a small prompt signal at m/z =44 shortly following the photolysis laser pulse, but thereafter the signals at m/z = 44 and 60 appear to be anti-correlated in time. The prompt signal could possibly originate from the reaction of a small amount of CH_3CH carbene formed during the photolysis process and a subsequent fast reaction with O_2 or from an analogous reaction to the minor yield of HCHO +IO in the corresponding $CH_2I + O_2$ reaction.[46, 47] A global analysis of the CH_3CHOO decays and CH_3CHO production yields a rate coefficient for reaction R9 of $k_9 = (1.3 \pm 0.3) \times 10^{-11}$ molecule^{-1} cm^{-3} s^{-1} with the large error (1σ) originating from a sensitivity of the fit to the prompt m/z = 44 production. The objective of product monitoring is not to determine a more precise or accurate value for k_9, but rather to

show that the data are consistent with direct production SO_3 from reaction R9. Using higher energy ionization photons at 13 eV, Taatjes et al.[1] were able to observe the direct production of SO_3 in their LFP/PIMS study of reaction R9, consistent with the observation of acetaldehyde in this work.

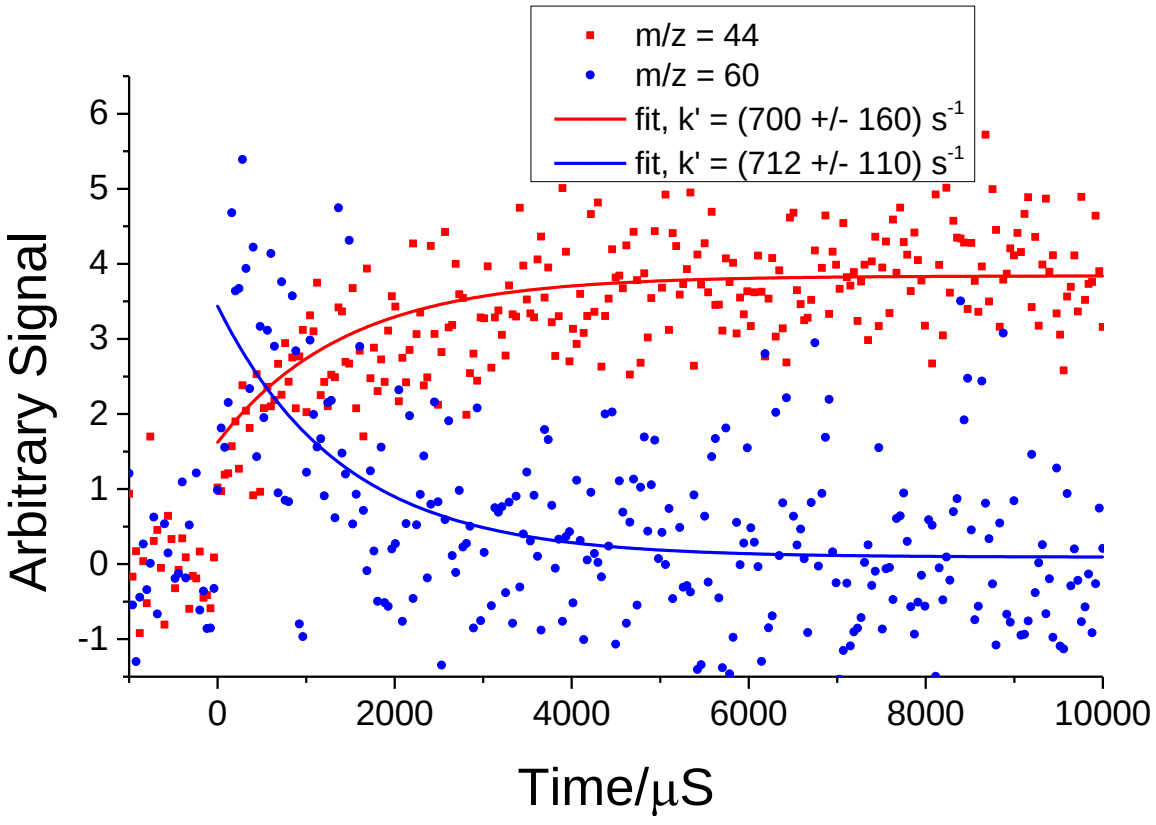

Fig. 6 A plot showing CH_3CHOO decay (m/z = 60, blue) and the simultaneous formation of a species at m/z = 44 (red), attributed to acetaldehyde. $[SO_2] = 3.2 \times 10^{13}$ cm^3 molecule^{-1} s^{-1}.

If reaction R9 occurs via a similar mechanism to the $CH_2OO + SO_2$ reaction, then at the low pressures of this study, one would expect 100% acetaldehyde production (R9a) with no stabilization component (R9b). Without a suitable titration reaction directly linking CH_3CHOO and CH_3CHO and with uncertainty as to the initial absolute $[CH_3CHOO]$, it is not possible to determine the yield of acetaldehyde accurately, however from the following arguments, we estimate that CH_3CHO is the dominant product. In the absence of SO_2, acetaldehyde was observed to form at rate equal to the intercept in Figure 5, ~150 s^{-1}. Assuming

that acetaldehyde is only formed from the self-reaction (second order kinetics) and not wall loss (first order kinetics), then our approximately exponential production of acetaldehyde limits the fraction of Criegee reacting via self-reaction to approximately 30%. This is consistent with a self-reaction rate coefficient of ~7×10^{-11} cm^3 $molecule^{-1}$ s^{-1} (CH_2OO self-reaction rate), a wall loss rate of 100 s^{-1} and $[CH_3CHOO]_0 \approx 7 \times 10^{11}$ molecule cm^{-3}. When a high $[SO_2]$ (> 3×10^{13} cm^3 $molecule^{-1}$ s^{-1}) is added to the system a greater fraction, ~75-90%, of CH_3CHOO reacts with SO_2. The resulting acetaldehyde signal is approximately three times greater than in the absence of SO_2, when only 30% of CH_3CHOO generates acetaldehyde, consistent with a majority of reaction R9 leading to acetaldehyde production (see supplementary information, section 5). This estimate of the dominance of $CH_3CHO + SO_3$ production at low pressures would be consistent with the calculations of Vereecken et al.[39] (>80 % $CH_3CHO + SO_3$ production at 4 Torr), however, Vereecken et al. show that at atmospheric pressure 97% of the secondary ozonide is collisionally stabilized.

Conclusions and Atmospheric Implications

The kinetics of the reaction of CH_2OO with SO_2 has been measured at (295 ± 2) K using laser flash photolysis to generate stabilized Criegee intermediate with the reaction being monitored by both photoionization mass spectroscopy and time-resolved UV absorption spectroscopy. The rate coefficients determined using both methods are in good agreement with a majority of the literature data and there is no evidence of enhancement of the rate coefficients under conditions of low SO_2 as proposed by Chhantyl-Pun et al.[26]

The rate coefficient for the reaction of CH_3CHI with oxygen is determined as $k_8 = (8.6 \pm 2.2) \times 10^{-12}$ cm^3 $molecule^{-1}$ s^{-1} and the yield of CH_3CHOO is determined as 0.86 ± 0.11 at 2 Torr of helium. The rate coefficient, k_8, is enhanced by a factor of ~4 from the equivalent C_1 reaction. The yield of I atom is lower than the equivalent C_1 process, as might be expected from a larger system where stabilization of the RIO_2* intermediate is expected to be relatively more efficient than I atom elimination.

The reaction of the C_2 Criegee, CH_3CHOO with SO_2, determined via LFP/PIMS, is slightly slower than the C_1 counterpart, in agreement with trends observed in other studies.[1, 29,

[42] The absolute rate coefficient for the reaction of CH_3CHOO with SO_2, $k_9 = (1.7 \pm 0.3) \times 10^{-11}$ cm^3 $molecule^{-1}$ s^{-1}, is in agreement with the recent study of Smith et al.[42] and close to that of Taatjes et al.[1] and Sheps et al.[29] Direct comparisons are not always appropriate as different experiments will have variable sensitivities to different conformers of the C_2 Criegee intermediate and there may be a pressure dependence. For reaction R9, a good correlation is observed between CH_3CHOO removal and CH_3CHO production and CH_3CHO is estimated to be the dominant product under our experimental conditions.

In the atmosphere, for syn-CH_3CHOO, reaction with either water dimer or monomer is expected to be slow. The rate coefficient with SO_2 is slightly lower than the C_1 equivalent, but is still fast enough that reaction R9 may still contribute to sulphate formation. For example, under relatively cool and dry conditions (relative humidity of 50%), reaction R9 could account for ~5% of C_2 Criegee removal, although reaction with water (monomer or dimer) are still the main processes for C_2 Criegee intermediate removal (see supplementary information, section 6, for further details). In addition to this, large discrepancies between modelled and measured H_2SO_4 concentrations in a Finnish boreal forest imply an unexpected increase in SO_2 oxidation. It has been postulated that this oxidation may be caused by CIs produced by monoterpene ozonolysis.[9] Indeed, one recent study suggests that on a regional scale, the impact that Criegee chemistry may have on [H_2SO_4] is significant,[48] and further work to investigate the kinetics, products and mechanisms of higher Criegee intermediates, particularly at higher pressures, is still required.

Acknowledgements

Funding from NERC providing studentships for NUMH, TRL and ZM and funding through grant NE/K005820/1 and Fellowship NE/L010798/1 for DS is gratefully acknowledged. We are grateful for useful discussions with Prof A. Orr-Ewing and Dr R. Chhantyal-Pun.

References

1. C. A. Taatjes, O. Welz, A. J. Eskola, J. D. Savee, A. M. Scheer, D. E. Shallcross, B. Rotavera, E. P. F. Lee, J. M. Dyke, D. K. W. Mok, D. L. Osborn and C. J. Percival, Science, 2013, **340**, 177-180.

2. O. Welz, A. J. Eskola, L. Sheps, B. Rotavera, J. D. Savee, A. M. Scheer, D. L. Osborn, D. Lowe, A. M. Booth, P. Xiao, M. A. H. Khan, C. J. Percival, D. E. Shallcross and C. A. Taatjes, Angew. Chem., Int. Ed., 2014, **53**, 4547-4550.

3. O. Welz, J. D. Savee, D. L. Osborn, S. S. Vasu, C. J. Percival, D. E. Shallcross and C. A. Taatjes, Science, 2012, **335**, 204-207.

4. D. L. Osborn and C. A. Taatjes, International Reviews in Physical Chemistry, 2015, **34**, 309-360.

5. D. Johnson and G. Marston, Chem. Soc. Rev., 2008, **37**, 699-716.

6. J. J. M. Lin and W. Chao, Chem. Soc. Rev., 2017, **46**, 7483-7497.

7. C. A. Taatjes, in Annual Review of Physical Chemistry, Vol 68, eds. M. A. Johnson and T. J. Martinez, Annual Reviews, Palo Alto, Editon edn., 2017, vol. 68, pp. 183-207.

8. Y. P. Lee, J. Chem. Phys., 2015, **143**, 020901.

9. R. L. Mauldin, T. Berndt, M. Sipila, P. Paasonen, T. Petaja, S. Kim, T. Kurten, F. Stratmann, V. M. Kerminen and M. Kulmala, Nature, 2012, **488**, 193-196.

10. H. F. Huang, A. J. Eskola and C. A. Taatjes, J. Phys. Chem. Lett., 2012, **3**, 3399-3403.

11. H. F. Huang, B. Rotavera, A. J. Eskola and C. A. Taatjes, J. Phys. Chem. Lett., 2013, **4**, 3824-3824.

12. D. Stone, M. Blitz, L. Daubney, T. Ingham and P. Seakins, Phys. Chem. Chem. Phys., 2013, **15**, 19119-19124.

13. D. Stone, M. Blitz, L. Daubney, N. U. M. Howes and P. Seakins, Phys. Chem. Chem. Phys., 2014, **16**, 1139-1149.

14. Y. Y. Wang, M. R. Dash, C. Y. Chung and Y. P. Lee, J. Chem. Phys., 2018, **148**, 064301.

15. Y. D. Liu, K. D. Bayes and S. P. Sander, J. Phys. Chem. A, 2014, **118**, 741-747.

16. L. Sheps, J. Phys. Chem. Lett., 2013, **4**, 4201-4205.

17. T. Berndt, J. Voigtlander, F. Stratmann, H. Junninen, R. L. Mauldin, M. Sipila, M. Kulmala and H. Herrmann, Phys. Chem. Chem. Phys., 2014, **16**, 19130-19136.

18. T. R. Lewis, M. A. Blitz, D. E. Heard and P. W. Seakins, Phys. Chem. Chem. Phys., 2015, **17**, 4859-4863.

19. M. C. Smith, C. H. Chang, W. Chao, L. C. Lin, K. Takahashi, K. A. Boering and J. J. M. Lin, J. Phys. Chem. Lett., 2015, **6**, 2708-2713.

20. L. C. Lin, H. T. Chang, C. H. Chang, W. Chao, M. C. Smith, C. H. Chang, J. J. M. Lin and K. Takahashi, Phys. Chem. Chem. Phys., 2016, **18**, 4557-4568.

21. R. Yajima, Y. Sakamoto, S. Inomata and J. Hirokawa, J. Phys. Chem. A, 2017, **121**, 6440-6449.

22. L. Sheps, B. Rotavera, A. J. Eskola, D. L. Osborn, C. A. Taatjes, K. Au, D. E. Shallcross, M. A. H. Khan and C. J. Percival, Phys. Chem. Chem. Phys., 2017, **19**, 21970-21979.

23. Y. Q. Liu, F. H. Liu, S. Y. Liu, D. X. Dai, W. R. Dong and X. M. Yang, Phys. Chem. Chem. Phys., 2017, **19**, 20786-20794.

24. W. Chao, J. T. Hsieh, C. H. Chang and J. J. M. Lin, Science, 2015, **347**, 751-754.

25. K. T. Kuwata, M. R. Hermes, M. J. Carlson and C. K. Zogg, J. Phys. Chem. A, 2010, **114**, 9192-9204.

26. R. Chhantyal-Pun, A. Davey, D. E. Shallcross, C. J. Percival and A. J. Orr-Ewing, Phys. Chem. Chem. Phys., 2015, **17**, 3617-3626.

27. M. T. Baeza-Romero, M. A. Blitz, A. Goddard and P. W. Seakins, Int. J. Chem. Kinet., 2012, **44**, 532-545.

28. M. A. Blitz, A. Goddard, T. Ingham and M. J. Pilling, Rev. Sci. Instrum., 2007, **78**, 034103.

29. L. Sheps, A. M. Scully and K. Au, Phys. Chem. Chem. Phys., 2014, **16**, 26701-26706.

30. N. U. M. Howes, J. P. A. Lockhart, M. A. Blitz, S. A. Carr, M. T. Baeza-Romero, D. E. Heard, R. J. Shannon, P. W. Seakins and T. Varga, Phys. Chem. Chem. Phys., 2016, **18**, 26423-26433.

31. C. A. Taatjes, Int. J. Chem. Kinet., 2007, **39**, 565-570.

32. T. Lewis, D. E. Heard and M. A. Blitz, Rev. Sci. Instrum., 2018, **89**, L024101.

33. W. L. Ting, C. H. Chang, Y. F. Lee, H. Matsui, Y. P. Lee and J. J. M. Lin, J. Chem. Phys., 2014, **141**, 104308.

34. D. Johnson, A. G. Lewin and G. Marston, The Journal of Physical Chemistry A, 2001, **105**, 2933-2935.

35. H. L. Huang, W. Chao and J. J. M. Lin, Proc. Natl. Acad. Sci. U. S. A., 2015, **112**, 10857-10862.

36. G. M. Handisides, C. Plass-Dulmer, S. Gilge, H. Bingemer and H. Berresheim, Atmos. Chem. Phys., 2003, **3**, 1565-1588.

37. W. L. Lin, X. B. Xu, Z. Q. Ma, H. R. Zhao, X. W. Liu and Y. Wang, Journal of Environmental Sciences, 2012, **24**, 34-49.

38. Z. J. Buras, R. M. I. Elsamra and W. H. Green, J. Phys. Chem. Lett., 2014, **5**, 2224-2228.

39. L. Vereecken, H. Harder and A. Novelli, Phys. Chem. Chem. Phys., 2012, **14**, 14682-14695.

40. A. Masaki, S. Tsunashima and N. Washida, J. Phys. Chem., 1995, **99**, 13126-13131.

41. A. J. Eskola, D. Wojcik-Pastuszka, E. Ratajczak and R. S. Timonen, Phys. Chem. Chem. Phys., 2006, **8**, 1416-1424.

42. M. C. Smith, W. L. Ting, C. H. Chang, K. Takahashi, K. A. Boering and J. J. M. Lin, J. Chem. Phys., 2014, **141**, 074302.

43. M. J. Newland, A. R. Rickard, M. S. Alam, L. Vereecken, A. Muñoz, M. Ródenas and W. J. Bloss, Phys. Chem. Chem. Phys., 2015, **17**, 4076-4088.

44. A. Novelli, L. Vereecken, J. Lelieveld and H. Harder, Phys. Chem. Chem. Phys., 2014, **16**, 19941-19951.

45. J. C. Traeger, R. G. McLoughlin and A. J. C. Nicholson, J. Am. Chem. Soc., 1982, **104**, 5318-5322.

46. S. Enami, T. Yamanaka, S. Hashimoto, M. Kawasaki, K. Tonokura and H. Tachikawa, Chem. Phys. Lett., 2007, **445**, 152-156.

47. E. S. Foreman and C. Murray, J. Phys. Chem. A, 2015, **119**, 8981-8990.

48. C. J. Percival, O. Welz, A. J. Eskola, J. D. Savee, D. L. Osborn, D. O. Topping, D. Lowe, S. R. Utembe, A. Bacak, G. M c Figgans, M. C. Cooke, P. Xiao, A. T. Archibald, M. E. Jenkin, R. G. Derwent, I. Riipinen, D. W. K. Mok, E. P. F. Lee, J. M. Dyke, C. A. Taatjes and D. E. Shallcross, Faraday Discussions, 2013, **165**, 45-73.